nature physics

Article

https://doi.org/10.1038/s41567-024-02486-0

Non-trivial quantum geometry and the strength of electron-phonon coupling

Received: 14 April 2023

Accepted: 26 March 2024

Published online: 27 May 2024

Check for updates

Jiabin Yu^{1,2}, Christopher J. Ciccarino ® ^{3,4}, Raffaello Bianco ® ^{5,6,7,8}, Ion Errea ® ^{5,9,10}, Prineha Narang ® ⁴ & B. Andrei Bernevig ® ^{1,10,11} ⊠

Electron–phonon coupling is crucial for the existence of various phases of matter, in particular superconductivity and density waves. Here, we devise a theory that incorporates the quantum geometry of the electron bands into the electron–phonon coupling, demonstrating the crucial contributions of the Fubini–Study metric or its orbital selective version to the dimensionless electron–phonon coupling constant. We apply the theory to two materials, that is, graphene and MgB $_2$, where the geometric contributions account for approximately 50% and 90% of the total electron–phonon coupling constant, respectively. The quantum geometric contributions in the two systems are further bounded from below by topological contributions. Our results suggest that the non-trivial electron band geometry or topology might favour superconductivity with a relatively high critical temperature.

Topology has been at the forefront of condensed matter physics for the past two decades, influencing our understanding of quantum materials and phenomena. More recently, it has however become clear and appreciated that a more general concept, that of quantum geometry. manifests itself in a series of quantum phenomena involving flat electronic bands. Non-trivial quantum geometry—expressing the change in wavefunctions under infinitesimal change in the Hamiltonian parameters such as momentum (Fig. 1b)—appears naturally in multi-band systems^{1,2}. If a band is topologically non-trivial, the quantum metric is bounded from below by the topological invariant of the band (Fig. 1e). However, even if the band is topologically trivial but has Wannier states that are not fully localized on the atoms (such as in the obstructed atomic limits³), the quantum geometry—usually described up to now by the Fubini–Study metric (FSM)—can be bounded from below (Fig. 1c,d). For flat electronic bands—whose flatness comes from quantum interference effects⁴⁻⁶ – it has been shown that the quantum geometry is directly related to various phenomena such as superfluid weight^{7,8}. Besides flat band systems, the effect of quantum geometry in dispersive band systems has also been studied (see, for example, refs. 9-22).

All previous works on quantum geometry either do not include a realistic interaction or treat the interaction strength as a tuning parameter. Up to now, it is unknown how quantum geometry (characterized by, for example, the FSM) affects the strength of realistic interactions. One main and important interaction in solids is the electron–phonon coupling (EPC), which is crucial for superconductivity $^{23-25}$ and other quantum phases. For phonon-mediated superconductors, a large λ typically leads to a high superconducting transition temperature $T_{\rm c}$ (refs. 26,27). Therefore, it is natural to ask how λ is directly related to the electron band geometry—most importantly to the Fermi surface quantum geometry (characterized by, for example, the FSM)—which is bounded by topology. Such a relation, if revealed, may help the search for new superconductors, given the large number of topological materials $^{28-30}$.

In this Article, we compute the contribution of the electron band geometry and topology to the bulk EPC constant λ . First, we introduce a simple (but in many cases remarkably accurate) model—dubbed the Gaussian approximation (GA)—for the EPC to show its deep link to the electronic band Hamiltonian. In this approximation, the quantum

¹Department of Physics, Princeton University, Princeton, NJ, USA. ²Condensed Matter Theory Center and Joint Quantum Institute, Department of Physics, University of Maryland, College Park, MD, USA. ³Department of Materials Science and Engineering, Stanford University, Stanford, CA, USA. ⁴College of Letters and Science, University of California, Los Angeles, CA, USA. ⁵Centro de Física de Materiales (CSIC-UPV/EHU), Donostia/San Sebastián, Spain. ⁶Ruder Bosković Institute, Zagreb, Croatia. ⁷Dipartimento di Scienze Fisiche, Informatiche e Matematiche, Università di Modena e Reggio Emilia, Modena, Italy. ⁸Centro S3, Istituto Nanoscienze-CNR, Modena, Italy. ⁹Fisika Aplikatua Saila, Gipuzkoako Ingeniaritza Eskola, University of the Basque Country (UPV/EHU), Donostia/San Sebastián, Spain. ¹⁰Donostia International Physics Center, Donostia/San Sebastián, Spain. ¹¹IKERBASQUE, Basque Foundation for Science, Bilbao, Spain. ¹²Ee-mail: bernevig@princeton.edu

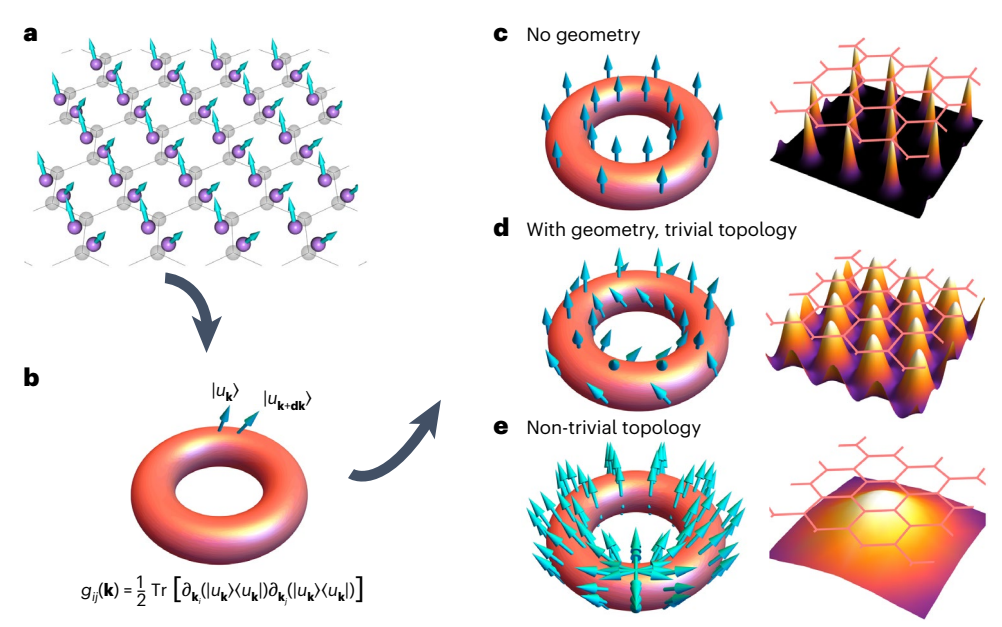


Fig. 1 | **Quantum geometry and EPC. a**, When the ions (purple) move away from the equilibrium positions (grey) owing to phonons, electrons (turquoise arrows) would follow the motions of ions in the tight binding approximation owing to EPC. **b**, The FSM $g_{ij}(\mathbf{k})$ provides a measure of quantum geometry, that is, how the periodic part of the Bloch state, $|u_{\mathbf{k}}\rangle$, varies in the first Brillouin zone (1BZ,

represented by the torus). \mathbf{c} , Quantum geometry can vanish (left) in the trivial atomic limit (right). \mathbf{d} , Quantum geometry must be strong (left) for the obstructed atomic limit (right), even if the band topology is trivial. \mathbf{e} , The non-trivial band topology forces the quantum geometry to be strong (left) and leads to power-law decayed Wannier functions (right).

geometric contribution to λ emerges naturally and can be differentiated from the energy dispersion contribution. In particular, we find that either the FSM or the orbital selective FSM (OFSM) directly enters the expression for the EPC. We show that, when the electron states on or near the Fermi surfaces exhibit topology—such as winding numbers of the wavefunctions—the geometric contribution (arising from the (O) FSM) is bounded from below by the topological contribution (arising from topological invariants). The topological contribution serving as a lower bound of the geometric contribution is in the same spirit as the band topology serving as a lower bound of the band geometry.

To test our theory, we apply it to the EPC of two famous materials, that is, graphene and MgB₂, where we find that our approximation becomes (almost) exact; we then identify the quantum geometric contributions to the bulk EPC constant λ , as well as the topological contributions that bound the geometric ones from below, in the two systems. We further perform ab initio calculations³¹, with two different methods for MgB₂, from which we find that the quantum geometric (topological) contribution to λ accounts for roughly 50% (50%) and 90% (43%) of the total value of the EPC constant in graphene and MgB₂, respectively. Beyond the GA, we introduce an alternative but similar way of identifying the quantum geometric contributions to λ based on the symmetry representations (reps) and the short-ranged nature of the hopping, and reproduce our results. Since MgB2 is a phonon-mediated superconductor with $T_c = 39 \text{ K}$ (refs. 32–34), our work on MgB₂ suggests that strong geometric properties or a non-trivial topology of the electron Bloch states may favour a strong EPC constant λ and thus a high superconducting T_c , which would serve as guidance for future searches for superconductors.

Gaussian approximation: geometric contribution to λ

The bulk EPC constant²⁶ $\lambda = 2 \int_0^\infty d\omega \frac{\alpha^2 F(\omega)}{\omega}$ is obtained from the Eliashberg function²⁵ $\alpha^2 F$. It can be written as $\lambda = 2 \frac{D(\mu)}{N} \frac{\hbar \langle \Gamma \rangle}{\hbar^2 \langle \omega^2 \rangle}$, where

 $D(\mu)$ is the single-particle electron density of states at the chemical potential μ , N is the number of lattice sites and $\langle \omega^2 \rangle$ is the McMillan

mean-squared phonon frequency. For a multi-band electron system, we show that the average phonon line width $\langle \Gamma \rangle$ (up to a factor of $D^2(\mu)$) is the average of

$$\Gamma_{nm}(\mathbf{k}_1, \mathbf{k}_2) = \frac{\hbar}{2} \sum_{\mathbf{\tau}, i} \frac{1}{m_{\mathbf{\tau}}} \operatorname{Tr} \left[P_n(\mathbf{k}_1) F_{\mathbf{\tau}i}(\mathbf{k}_1, \mathbf{k}_2) P_m(\mathbf{k}_2) F_{\mathbf{\tau}i}^{\dagger}(\mathbf{k}_1, \mathbf{k}_2) \right]$$
(1)

over the Fermi surfaces. \mathbf{k}_1 and \mathbf{k}_2 are the Bloch momenta of electrons, $\boldsymbol{\tau}$ is the sub-lattice vector, $m_{\boldsymbol{\tau}}$ is the mass of the ion at $\boldsymbol{\tau}$, i labels the spatial directions of the possible ion motions and crucially $P_n(\mathbf{k}) = U_n(\mathbf{k})U_n^{\dagger}(\mathbf{k})$ is the projection matrix to the nth electron band with $U_n(\mathbf{k})$ the eigenvector. $F_{\tau i}(\mathbf{k}_1, \mathbf{k}_2)$ in equation (1) is the EPC matrix in the electron atomic basis and the ion motion basis, whose general expression can be found in equation (B41) in Supplementary Section B. As embedded in three-dimensional (3D) space, the ion can move in three dimensions (that is, i = x, y, z), regardless of the sample dimensionality.

For time reversal (TR)-invariant systems with negligible Coulomb interaction, we show in Supplementary Section E that the mean-field superconducting $k_{\rm B}T_{\rm c} \ge 1.13\epsilon_{\rm c}{\rm e}^{-\bar{\lambda}}$ is bounded from below by λ regardless of the pairing function, as long as (1) the cutoff ϵ_c is much larger than the temperature and (2) the bands cut by the Fermi energy are dispersive with a large Fermi velocity. (We note that the bound relies on the Migdal-Eliashberg theory, which usually holds in the weak coupling regime. The Migdal-Elishberg theory is not necessarily reliable in the strong coupling regime 35,36 .) If the Coulomb interaction is considerable, the T_c of phonon-mediated superconductors still typically increases with increasing λ (refs. 26,27). In the expression for λ , $\langle \omega^2 \rangle$ can be well approximated by certain phonon frequencies in many cases (for example, in graphene and MgB₂) and $D(\mu)$ only involves electrons. Thus, the main information regarding the EPC is often in the average phonon line width $\langle \Gamma \rangle$. To study $\langle \Gamma \rangle$, we adopt the two-centre approximation³⁷ for the EPC: only the relative motions of two ions matter for the EPC between the electronic orbitals on those two ions. As a result, the EPC matrix $F_{\tau i}(\mathbf{k}_1, \mathbf{k}_2)$ has the form (Supplementary Section C)

$$F_{\mathbf{\tau}i}(\mathbf{k}_1, \mathbf{k}_2) = \chi_{\mathbf{\tau}} f_i(\mathbf{k}_2) - f_i(\mathbf{k}_1) \chi_{\mathbf{\tau}}, \tag{2}$$

where χ_{τ} is a diagonal projection matrix with elements being 1 only for the electron degrees of freedom (such as orbitals) at τ . $f_i(\mathbf{k})$ is a matrix for the case with more than one bands and is the quantity we want to determine (Supplementary Section C), whose deep physical origin is missing in the literature.

We now show that $f_i(\mathbf{k})$ is intimately related to the electronic Hamiltonian. To show this general relation, we introduce the GA. As a concrete simple illustration, we consider a 3D system with only one kind of atom and one spinless s orbital per atom (for a generalization, see Supplementary Sections F and H). We allow multiple atoms per unit cell so that more than one electron band can exist. Under the two-centre approximation, the non-interacting electron Hamiltonian and EPC Hamiltonian are directly given by the smooth hopping function $t(\mathbf{r})$, which specifies the hopping between two s orbitals separated by r. Explicitly, the electron matrix Hamiltonian reads $[h(\mathbf{k})]_{\tau\tau'} = \sum_{\mathbf{R}} f(\mathbf{R} + \mathbf{\tau} - \mathbf{\tau}') e^{-i\mathbf{k}\cdot(\mathbf{R} + \mathbf{\tau} - \mathbf{\tau}')}$ with **R** labelling the lattice vectors, and the EPC $f_i(\mathbf{k})$ in equation (2) reads $\left[f_i(\mathbf{k})\right]_{\mathbf{\tau}_1\mathbf{\tau}_2} = \sum_{\mathbf{R}} \mathrm{e}^{-\mathrm{i}\mathbf{k}\cdot(\mathbf{R}+\mathbf{\tau}_1-\mathbf{\tau}_2)} \left.\partial_{r_i}t(\mathbf{r})\right|_{\mathbf{r}=\mathbf{R}+\mathbf{\tau}_1-\mathbf{\tau}_2}$. The GA assumes the hopping function to have a Gaussian form: $t(\mathbf{r}) = t_0 \exp\left[\gamma \frac{|\mathbf{r}|^2}{2}\right]$, where y < 0 is determined by the standard deviation. Usual overlaps between orbitals in lattices do have an exponentially decaying form, hence we expect the GA to be a qualitatively and quantitatively good description of the physics. Other powers of $|\mathbf{r}|$ in the exponential are possible and lead to generalized quantum geometric quantities, but we focus on the GA owing to its simplicity. We later show it is exact in the short-range hopping or **k**·**p** models of graphene and MgB₂.

Crucially, the GA enables us to uncover a relation between the EPC $f_i(\mathbf{k})$ and the electron Hamiltonian $h(\mathbf{k})$. As $\partial_{r_i} t(\mathbf{r}) = \gamma r_i t(\mathbf{r})$, we Fourier transform to find a simple relation between the EPC and the electron Hamiltonian

$$f_i(\mathbf{k}) = i\gamma \partial_{k_i} h(\mathbf{k}). \tag{3}$$

With the spectral decomposition $h(\mathbf{k}) = \sum_n E_n(\mathbf{k}) P_n(\mathbf{k})$, where $E_n(\mathbf{k})$ is the nth electron band with projection operator $P_n(\mathbf{k})$, we can split the EPC $f_i(\mathbf{k})$ into energetic and geometric parts $f_i(\mathbf{k}) = f_i^E(\mathbf{k}) + f_i^{geo}(\mathbf{k})$, where

$$f_i^{E}(\mathbf{k}) = i\gamma \sum_n \partial_{k_i} E_n(\mathbf{k}) P_n(\mathbf{k}),$$

$$f_i^{geo}(\mathbf{k}) = i\gamma \sum_n E_n(\mathbf{k}) \partial_{k_i} P_n(\mathbf{k}).$$
(4)

 $f_i^{\rm E}({\bf k})$ is the energetic part of the EPC since it vanishes if electron bands are exactly flat. $f_i^{\rm geo}({\bf k})$ is the geometric part of the EPC since $f_i^{\rm geo}({\bf k})$ relies on the momentum dependence of $P_n({\bf k})$; it vanishes for trivial bands with no ${\bf k}$ dependence in their eigenstates or for one-band systems. The separation in equation (4) allows us the split the bulk EPC λ into three parts as $\lambda=\lambda_{\rm E}+\lambda_{\rm geo}+\lambda_{\rm E-geo}$, where $\lambda_{\rm E}$ is linked to $f_i^{\rm E}({\bf k})$, $\lambda_{\rm geo}$ to $f_i^{\rm geo}({\bf k})$, and $\lambda_{\rm E-geo}$ to both $f_i^{\rm E}({\bf k})$ and $f_i^{\rm geo}({\bf k})$. Similar to the names of $f_i^{\rm E}({\bf k})$ and $f_i^{\rm geo}({\bf k})$, we call $\lambda_{\rm E}$ and $\lambda_{\rm geo}$ the energetic and geometric contributions to the bulk EPC constant λ , respectively. $\lambda_{\rm E-geo}$ is not our focus in this work since it vanishes in graphene and MgB2 under the approximation that we adopt, though $\lambda_{\rm E-geo}$ also has geometric dependence in it (Supplementary Section A).

In particular, $f_i^{\text{geo}}(\mathbf{k})$ is responsible for leading to the (O)FSM in $\lambda_{\text{geo}} = \lambda_{\text{geo,1}} + \lambda_{\text{geo,2}}$, where both parts depend on geometric quantities, as discussed in Supplementary Section A. In this work, we mainly focus on $\lambda_{\text{geo,1}}$, since $\lambda_{\text{geo,2}}$ is restricted to zero by symmetries for graphene and is either restricted to zero or can be converted to the same geometric expressions as $\lambda_{\text{geo,1}}$ for MgB₂, as discussed in the next section. Explicitly, in the two-band case, $\lambda_{\text{geo,1}}$ reads

$$\lambda_{\text{geo},1} = \frac{2\Omega \gamma^2}{(2\pi)^3 m \langle \omega^2 \rangle} \sum_{n,i,\tau} \int_{FS_n} d\sigma_{\mathbf{k}} \frac{\Delta E^2(\mathbf{k})}{|\nabla_{\mathbf{k}} E_n(\mathbf{k})|} a_{\tau} [g_{n,\tau}(\mathbf{k})]_{ii}, \quad (5)$$

where m is the mass of the ion, Ω is the volume of the unit cell, $d\sigma_{\mathbf{k}}$ is the measure on the Fermi surface, $\Delta E(\mathbf{k})$ is the difference between two energy bands, FS_n is the Fermi surface given by $E_n(\mathbf{k}) = \mu$ and $a_{\tau} = \frac{1}{D(\mu)} \sum_m \sum_{\mathbf{k}_2}^{\text{IBZ}} \delta(\mu - E_m(\mathbf{k}_2)) \left[P_m(\mathbf{k}_2) \right]_{\tau \tau} \text{(Supplementary Section A)}.$

$$\left[g_{n,\tau}(\mathbf{k})\right]_{ij} = \frac{1}{2} \operatorname{Tr}\left[\partial_{k_i} P_n(\mathbf{k}) P_n(\mathbf{k}) \partial_{k_j} P_n(\mathbf{k}) \chi_{\tau}\right] + (i \leftrightarrow j) \tag{6}$$

is the OFSM. More general definitions of the OFSM can be found in Supplementary Section G, and similar OFSM generalizations were proposed in ref. 38. When symmetries require a_{τ} to be the same for all τ (as in graphene), the OFSM would be summed over all τ and would reduce to the conventional FSM.

Although we only discuss the GA for a 3D system with only one kind of atom and one spinless s orbital per atom, the GA can be defined for more complicated cases. We also introduce an alternative way of identifying the geometric contribution to λ on the basis of the symmetry reps for systems with short-range hoppings (Supplementary Section D). Both methods can be applied to graphene and MgB $_2$ and give identical results. Moreover, we also use the most general symmetry-allowed short-range hopping form to reproduce the results from GA in graphene and MgB $_2$.

We have not developed a completely general version of the GA that is applicable to all systems. In general, it is unlikely to cover the full ab initio results just by allowing other powers of the distance between orbitals in the exponential or in the prefactor of the exponential. Allowing other powers of the distance can cover the radial part of the EPC, that is, the EPC matrix elements that correspond to the atomic motions parallel to the hopping direction; however, it cannot always cover the angular part of the EPC, that is, the EPC matrix elements from the atomic motions perpendicular to the hopping direction, which might be considerable when the orbitals have strong angular dependence, such as p, d and f orbitals. As discussed in the next section, graphene is special since p_z orbitals are effectively s orbitals in two dimensions, and we only need to consider the in-plane motions to the leading order, which therefore involve no angular dependence; MgB₂ is also special since the angular part of the EPC has the same expression as the radial part of the EPC to the leading order, which would allow us to use the GA with additional powers in the prefactor to cover the whole EPC to the leading order. Nevertheless, this is not always true in general. Therefore, when studying the geometric contribution to EPC in other systems, one might need certain modification of equation (3) beyond what we will do for graphene and MgB₂ in the rest of this paper and might also need to verify the results with different methods. Nevertheless, it is, in many case, possible to use certain polynomials of r to re-express the spatial gradient of the hopping functions, which, when the hopping is short-ranged enough, would give momentum derivatives of the electron Hamiltonian after the Fourier transformation and give geometric contribution.

Geometric contribution to λ in graphene and MgB₂

We now apply the GA to the specific cases of graphene and MgB_2 . With the nearest-neighbour (NN) hopping model of graphene³⁹, we find that the EPC form (equation (3)) derived from the GA is exact in graphene for in-plane atom motions. Owing to the mirror symmetry that flips the z direction, the out-of-plane atomic motions do not couple to the electrons, thus we find that the energetic and geometric parts of the EPC for graphene in equation (4) are non-zero only for in-plane i=x,y. Then, we obtain (Supplementary Section F)

$$\lambda_{\rm E} = \frac{\Omega \gamma^2}{(2\pi)^2 m_{\rm C} \langle \omega^2 \rangle} \int_{\rm FS} d\sigma_{\bf k} |\nabla_{\bf k} E_{n_{\rm F}}({\bf k})|,$$

$$\lambda_{\rm geo} = \frac{\Omega \gamma^2}{(2\pi)^2 m_{\rm C} \langle \omega^2 \rangle} \int_{\rm FS} d\sigma_{\bf k} \frac{\Delta E^2({\bf k})}{|\nabla_{\bf k} E_{n_{\rm F}}({\bf k})|} {\rm Tr} \left[g_{n_{\rm F}}({\bf k}) \right],$$
(7)

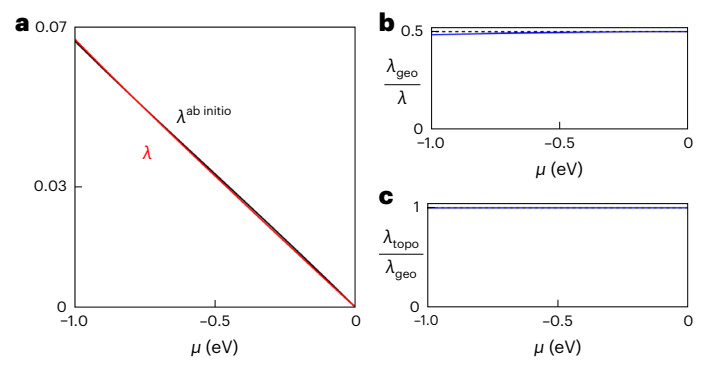


Fig. 2 | **Plots for graphene.** The chemical potential μ ranges from -1 eV to 0 eV, while setting the Dirac point energy to be zero. **a**, A plot of the EPC constants from the ab initio calculations (λ ^{ab initio}, black) and from equation (7) (λ , red). **b**,**c**, Plots of $\lambda_{\rm geo}/\lambda$ (**b**) and $\lambda_{\rm topo}/\lambda$ (**c**).

where $m_{\rm C}$ is the mass of a carbon atom, $E_{n_{\rm F}}({\bf k})$ is the band that gives the Fermi surface and $\Delta E(\mathbf{k})$ is the absolute difference of two energy bands. Remarkably, we find that, as advertised, the FSM of the electron Bloch states $-[g_n(\mathbf{k})]_{ii} = \text{Tr}[\partial_{k_i} P_n(\mathbf{k}) \partial_{k_i} P_n(\mathbf{k})]/2$ (equal to the expression in Fig. 1b under the tight binding approximation)—directly appears in λ_{geo} . The appearance of the FSM in equation (7) comes from $a_{\tau} = 1/2$ in equation (5) and $\lambda_{geo.2}$ = 0 for graphene, owing to the $C_2\mathcal{T}$ and C_3 symmetry, respectively, where C_n is the *n*-fold rotational symmetry around the z axis and \mathcal{T} is the TR symmetry. The symmetries of graphene also require that $\lambda_{E-geo} = 0$. Therefore, the bulk EPC constant λ of graphene only has the energetic and geometric contributions in equation (7), that is, $\lambda = \lambda_F + \lambda_{geo}$ (Supplementary Section F). Analytically, we find (Supplementary Section F) that λ_{geo}/λ limits to exactly 50% as μ approaches the energy of the Dirac points (which is zero). Remarkably, half of the EPC strength is supported by the geometric (and as we will show, topological) properties of the graphene Bloch states.

We determine the numerical values of the model parameter γ (in addition to the electron NN hopping and $\langle \omega^2 \rangle$) by matching our model to our ab initio calculation (Supplementary Section I). With the values of the model parameters (Supplementary Section F), we find that λ from our model almost perfectly matches with that from the ab initio calculation for a large range of μ up to -1 eV, as shown in Fig. 2a. We note that we do not tune the EPC parameter γ to fit our analytical λ to our $\lambda^{ab \, \text{initio}}$; instead, we determine the value of γ by matching the EPC analytic or ab initio matrix elements at the corners of the 1BZ. The match in Fig. 2a is hence not a result of tuning the EPC parameter and shows the great validity of the our GA. Moreover, our numerical calculation also finds that the geometric contribution is roughly 50% of the total λ (Fig. 2b), consistent with our analytical results. In Fig. 2a, we directly use the value of $\langle \omega^2 \rangle$ from the ab initio calculation. We find that $\langle \omega^2 \rangle$

can be approximated by an analytical expression $\langle \omega^2 \rangle = \frac{2\omega_{E_{2g}}^2(\Gamma)\omega_{\Lambda_1'}^2(K)}{\omega_{E_{2g}}^2(\Gamma) + \omega_{\Lambda_1'}^2(K)}$

(derived for $\mu \to 0$) with only 9% error, where $\omega_{E_{2g}}(\Gamma)$ and $\omega_{A_1'}(K)$ are the frequencies of the E_{2g} phonons at Γ and the A_1' phonons at K, respectively (Supplementary Section F). This underscores the excellent agreement of our analytic calculation with realistic ab initio.

Although the direct application of GA is not straightforward for a moiré system (which we leave for future work), we indeed find that the mean-field critical temperature of twisted bilayer graphene derived from the EPC can be estimated by a geometric expression similar to equation (7) in the first chiral limit 40,41 based on the topological heavy fermion framework 42,43 (see Supplementary Section F for details). Our approximated expression relies on the FSM of the flat bands and gives $T_c \approx 0.6$ K around the magic angles, which is close to the experimental values 44.

While graphene is a relatively 'simple' compound and one could discount our excellent agreement and the findings that follow as accidental, MgB $_2$ (Fig. 3a) is a far more complicated system 32 with multiple Fermi surfaces. The EPC constant λ only involves electron states at the Fermi energy, which originate from B atoms 45 (Fig. 3b). In addition, the main phonon contribution to λ is from the E_2 modes along Γ –A (enhanced to E_{2g} exactly at Γ and A), which also only involve B atoms 46 (Fig. 3a). The irrelevance of Mg for λ is supported by ref. 34, which finds an isotope effect of Mg atoms much smaller than that of the B atoms. Therefore, we neglect Mg atoms when constructing the models for electrons and EPC.

The bands near the Fermi level originate from the σ bonding among $B \rho_x/\rho_y$ orbitals and the π bonding among $B \rho_z/\rho_y$ orbitals and the π bonding among $B \rho_z$ orbitals 45 (Fig. 3b). The Fermi surfaces of the two types of bonding are separated from each other by a large in-plane momentum difference (Supplementary Section H), while the dominant phonon modes for λ (mainly the E_2 phonons along Γ -A that are enhanced to E_{2g} at Γ and A) have small in-plane phonon momenta 47 . Therefore, for evaluating λ , we reasonably assume that the σ bonding states are decoupled from the π bonding states in the electron and EPC Hamiltonian, which is also supported by the small line widths of the phonons with large in-plane momenta observed in ref. 48. As a result, we have $\lambda = \lambda_\pi + \lambda_\sigma$, where λ_π (λ_σ) is the EPC constant of the π bonding (σ bonding) states.

The derivation for λ_{π} is similar to the case of graphene, since the π bonding states originate from the p_z orbitals of B atoms arranged as AA stacked graphite (Fig. 3a). The main difference is that the π bonding states in MgB₂ have an extra NN hopping along the z direction in our model, which mainly affects the energetic contribution $\lambda_{\pi F}$. Nevertheless, we can still use the GA in the x and y directions to derive the energetic and geometric parts of the EPC, which turns out to be the same as equation (4) except that the hopping decay $\gamma_{\pi,z}$ along z is different from $\gamma_{\pi,\parallel}$ along x or y. We adopt the GA only in the x-y plane because the dominant E_2 phonons arise from the in-plane (x-y) motions of the B atoms⁴⁷; the EPC Hamiltonian derived from the GA exactly matches the actual EPC Hamiltonian with NN terms for the in-plane atomic motions. We then find that $\lambda_{\pi} = \lambda_{\pi,F} + \lambda_{\pi,geo}$, where $\lambda_{\pi,F-geo}$ is zero again owing to symmetries. The geometric $\lambda_{\pi,geo}$ has the same form as λ_{geo} in equation (7) for graphene (relying on FSM), and $\lambda_{\pi,F}$ just acquires an extra derivative of dispersion with respective to k_z compared with λ_E in equation (7) for graphene, in addition to an extra factor $D_{\pi}(\mu)/D(\mu)$ in $\lambda_{\pi,E}$ and $\lambda_{\pi,geo}$ with $D_{\pi}(\mu)$ the density of the π bonding states (Supplementary Section H).

We now discuss λ_{σ} for the σ bonding states. By adopting the GA in the x and y directions and the NN hopping approximation along z, we obtain the energetic and geometric parts of the EPC, which are

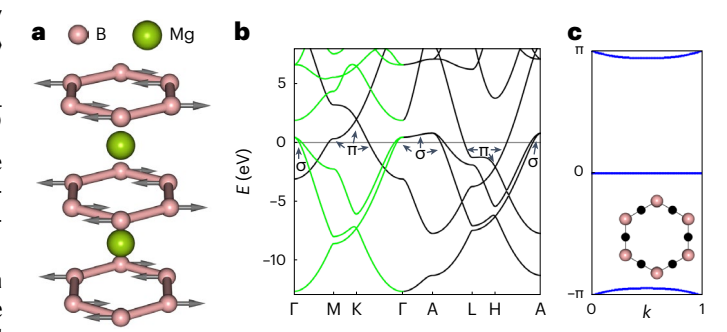


Fig. 3 | **Plots for MgB₂. a**, The structure of MgB₂. The grey arrows show one type of ion motion of the E_{2g} phonon at Γ. **b**, The ab initio band structure. σ and π indicate states from σ (p_x/p_y orbitals) and π -bonding (p_z orbital) among B atoms, respectively ⁴⁵. Green lines represent bands in the m_z -even subspace on the k_z = 0 plane. The Fermi energy is at 0. **c**, the Wilson loop spectrum of the lowest three bands in the m_z -even subspace on the k_z = 0 plane in **b**. The black dots in the inset show the Wannier centre of the three bands in one plane of B atoms (pink).

equal to equation (4) after replacing y by $\gamma_{\sigma,z}$ for the z direction and by $\gamma_{\sigma,\parallel}$ for the x and y directions (Supplementary Section H). The form of the EPC derived from the GA is exact if (1) we only include the NN hopping terms among p_x/p_y orbitals in the x and y plane and along z and (2) we only keep first order in \mathbf{k}_{\parallel} in the electron Hamiltonian (allowed by the small \mathbf{k}_{\parallel} on the Fermi surface of the σ bonding states shown in Fig. 3b). Because of the approximation to first order in \mathbf{k}_{\parallel} , the effective Hamiltonian has two doubly degenerate energy bands $E_{\mathrm{eff},n}(\mathbf{k})$ with n=1, 2—the lower $E_{\mathrm{eff},1}(\mathbf{k})$ is cut by the Fermi energy. While the effective model does not capture the splitting between the two bands near the Fermi level away from Γ -A shown in Fig. 3b, it is a good approximation for the evaluation of the EPC, as discussed at the end of this section and in Supplementary Section H.

Owing to the approximation to first order in \mathbf{k}_{\parallel} of the electron Hamiltonian, we find that $\lambda_{\sigma,E-geo}=0$ and thus obtain $\lambda_{\sigma}=\lambda_{\sigma,E}+\lambda_{\sigma,geo}$, which read

$$\lambda_{\sigma,E} = \frac{D_{\sigma}(\mu)}{D(\mu)} \frac{\gamma_{\sigma,z}^{2} \Omega}{(2\pi)^{3} m_{B} \langle \omega^{2} \rangle} \int_{FS_{eff,1}} d\sigma_{k} \frac{\left[\partial_{k_{z}} E_{eff,1}(\mathbf{k})\right]^{2}}{\left|\nabla_{k} E_{eff,1}(\mathbf{k})\right|}$$

$$\lambda_{\sigma,geo} = \frac{D_{\sigma}(\mu)}{D(\mu)} \frac{\gamma_{\sigma,\parallel}^{2} \Omega}{(2\pi)^{3} m_{B} \langle \omega^{2} \rangle} \int_{FS_{eff,1}} d\sigma_{k}$$

$$\times \sum_{i=x,y} \sum_{\alpha}^{-} \frac{\Delta E_{eff}^{2}(0) \left[g_{eff,1,\alpha}(0)\right]_{ii}}{\left|\nabla_{k} E_{eff,1}(\mathbf{k})\right|}$$
(8)

where $m_{\rm B}$ is the mass of the B atom, $\Delta E_{\rm eff}({\bf k}_{\parallel})$ is the absolute difference between two doubly degenerate bands of the effective model, $D_{\sigma}(\mu)$ is the density of the σ bonding states, and FS_{eff,1} is the Fermi surface given by $E_{\rm eff,1}({\bf k}) = \mu$. Also, $g_{\rm eff,1,\alpha}({\bf k}_{\parallel})$ is an OFSM

$$\begin{split} \left[g_{\mathrm{eff,1,\alpha}}(\mathbf{k}_{\parallel})\right]_{ij} &= \frac{1}{2}\mathrm{Tr}\left[\xi_{\alpha}\xi_{\alpha}^{\dagger}\partial_{k_{i}}P_{\mathrm{eff,1}}(\mathbf{k}_{\parallel})P_{\mathrm{eff,1}}(\mathbf{k}_{\parallel})\partial_{k_{j}}P_{\mathrm{eff,1}}(\mathbf{k}_{\parallel})\right] \\ &+ (i \leftrightarrow j), \end{split} \tag{9}$$

where ξ_{α} is a normalized vector that represents the electronic orbital linear combination picked by the relevant phonons for the EPC λ (Fig. 3a), and $P_{\rm eff,l}({\bf k}_{\parallel})$ is the projection matrix for the band $E_{\rm eff,l}({\bf k})$. In $\lambda_{\sigma,{\rm geo}}$, we only sum α over the parity-odd combinations of p_x/p_y orbitals (as indicated by the bar over the summation), because only the E₂ phonons matter under the approximation to first order in \mathbf{k}_{\parallel} of the electron Hamiltonian, and they flip the parity of the parity-even $P_{\text{eff,l}}(0)$. We only have the OFSM in $\lambda_{\sigma,geo}$ because $\lambda_{geo,2}$ mentioned above equation (5) (which, in general, might lead to a geometric quantity different from the OFSM) turns out to have the same final expression as the OFSM under the approximation of the linear-momentum electron Hamiltonian, which allows us to use the OFSM to describe the geometric dependence in $\lambda_{\text{geo},2}$ (Supplementary Section H). We only consider the OFSM and $\Delta E_{\rm eff}(\mathbf{k}_{\parallel})$ with $\mathbf{k}_{\parallel} = 0$ in equation (8) because the EPC matrix is given by the momentum derivative of the first order in \mathbf{k}_{\parallel} electron matrix Hamiltonian and thus is only reliable to zeroth order in \mathbf{k}_{\parallel} . We expect λ_{qF} to be small, as it does not involve in-plane motions of B atoms manifested by the absence of momentum derivative along x and y in the numerator (confirmed by our ab initio calculation).

We determine the hopping decay parameters $\gamma_{\pi,\parallel}, \gamma_{\pi,z}, \gamma_{\sigma,\parallel}$ and $\gamma_{\sigma,z}$ by matching the EPC $\Gamma_{nm}(\mathbf{k},\mathbf{k}+\mathbf{q})$ (with $\mathbf{k}=\Gamma$, K and \mathbf{q} along Γ –A) to our two ab initio calculations for MgB₂ (Supplementary Section H). Then, we obtain the values of various contributions to λ as shown in Table 1. Note that we do not tune $\gamma_{\pi,\parallel}, \gamma_{\pi,z}, \gamma_{\sigma,\parallel}$ and $\gamma_{\sigma,z}$ to fit our λ (a single value) to the single value $\lambda^{ab \text{ initio}}$ given by the ab initio calculation. Therefore, our value of λ = 0.78, which is remarkably close to the ab initio value $\lambda^{ab \text{ initio}}$ = 0.67 (17% error), verifies the validity of our approximations. Moreover, λ_{σ} is much larger than λ_{π} , which is consistent with the previous result⁴⁷.

Table 1 | Numerical values of λ and its various contributions for MqB.

λ (λ ^{abinitio})	0.78 (0.67)	λπ	0.16	λ_{σ}	0.62
$\lambda_{\scriptscriptstyle E}$	0.07	$\lambda_{\pi,E}$	0.07	$\lambda_{\sigma,E}$	0.00
$\lambda_{ m geo}$	0.71	$\lambda_{\pi, geo}$	0.09	$\lambda_{\sigma,geo}$	0.62
λ_{topo}	0.32	$\lambda_{\pi, \text{topo}}$	0.01	$\lambda_{\sigma, \mathrm{topo}}$	0.31

 $\lambda^{\text{abinitio}}$ = 0.67 in parentheses is the ab initio value for λ . All other values are calculated from our model with parameter values determined by matching the EPC $\Gamma_{nm}(\mathbf{k}, \mathbf{k} + \mathbf{q})$ (with $\mathbf{k} = \Gamma, K$ and \mathbf{q} along Γ -A) and fitting the electron band structure to the ab initio results. We do not fit the single value λ to $\lambda^{\text{abinitio}}$.

We find that the quantum geometric contribution is about 92% of the total λ , with most originating from the σ bonding. On the other hand, we find the energetic contribution from the σ bonding $(\lambda_{\sigma,E})$ to be negligible, consistent with our analytical argument. Therefore, the quantum geometry of the σ bonding states supports the large EPC constant in MgB₂. The values in Table 1 are calculated with the ab initio value of $\langle \omega^2 \rangle$ ($\hbar \sqrt{\langle \omega^2 \rangle} = 68$ meV), which can be approximated by the frequency of the E_{2g} phonons at Γ ($\hbar \omega_{E_{2g}}(\Gamma) = 75.3$ meV) with about 10% error.

Topological contributions to λ in graphene and MgB₂

The quantum geometric contributions in graphene and MgB $_2$ can be bounded from below by the topological invariants of the states on or near the Fermi surfaces in these materials, showing a deep connection between EPC and topology. The graphene $\lambda_{\rm geo}$ in equation (7) is bounded from below by the topological contribution $\lambda_{\rm topo}$, that is, $\lambda_{\rm geo} \geq \lambda_{\rm topo}$, where $\lambda_{\rm topo}$ reads

$$\lambda_{\text{topo}} = \frac{\Omega \gamma^2}{4m_{\text{C}} \langle \omega^2 \rangle} \frac{\left(|W_{\text{K}}| + |W_{\text{K}'}| \right)^2}{\int_{\text{FS}} d\sigma_{\mathbf{k}} \frac{|\nabla_{\mathbf{k}} E_n(\mathbf{k})|}{\Delta F^2(\mathbf{k})}},\tag{10}$$

where the chemical potential is moderate (for example, within 1 eV from 0). We derive equation (10) from the $f_{FS} d\sigma_k \sqrt{\text{Tr}\left[g_{n_F}(\mathbf{k})\right]} \geq \pi(|W_K| + |W_{K'}|)$ for moderate chemical potential. λ_{topo} is topological because $W_K = 1$ and $W_{K'} = -1$ are the integer winding numbers³⁹ (or chiralities) of the Dirac cones at K and K', respectively. Other parameters in equation (10) are defined below equation (7). We analytically show that $\lambda_{\text{topo}}/\lambda_{\text{geo}}$ limits to exactly 1 as $\mu \rightarrow 0$, which is consistent with the numerical calculation in Fig. 2c (Supplementary Section F).

For the π bonding states in MgB₂, the band structure has two \mathcal{PT} -protected nodal lines (where \mathcal{P} and \mathcal{T} are the inversion and TR symmetries) along k_z -directional hinges of the 1BZ, which carry winding numbers just like Dirac cones of graphene⁴⁹. The winding numbers account for the topological contribution $\lambda_{\pi,\text{topo}}$ to λ_{π} , which bounds the geometric $\lambda_{\pi,\text{geo}}$ from below in a similar way to equation (10) (Supplementary Section H).

Besides the nodal lines, we find an obstructed atomic set of bands on the k_z = 0 plane of MgB₂, which contains the σ bonding states around the Fermi level. The Bloch Hamiltonian has the mirror symmetry m_z (that flips the z direction) on the k_z = 0 plane. In the m_z -even subspace, we find that the isolated set of three bands cut by the Fermi energy is the elementary band representation $A_{\rm ig}$ @3f, which is obstructed atomic since the atoms are not at 3f and which have nonzero \mathcal{PT} -protected second Stiefel–Whitney class w_2 = 1 (Fig. 3c). (Here we follow the conventions of the Bilbao Crystallographic Server^{3,50}; a general discussion on w_2 can be found in ref. 51.) w_2 = 1 can be understood as having a band inversion at Γ , resulting in the effective Euler number $\Delta \mathcal{N} = 1$ of the σ bonding states around Γ near the Fermi level (see details in Supplementary Section H). Remarkably, the effective Euler number

 $\Delta\mathcal{N}=1$ gives a topological $\lambda_{\sigma,topo}$ that bounds the geometric contribution from below, where $\lambda_{\sigma,topo}$ reads

$$\lambda_{\sigma,\text{topo}} = \frac{D_{\sigma}(\mu)}{D(\mu)} \frac{4\pi \gamma_{\sigma,\parallel}^2 \Omega}{m_{\text{B}} \langle \omega^2 \rangle c^2} [\Delta \mathcal{N}]^2 \times \left[\int_{\text{FS}_{\text{eff,1}}} d\sigma_k \frac{|\nabla_k E_{\text{eff,1}}(\mathbf{k})|}{|\mathbf{d}(\mathbf{k}_{\parallel})|^2} \right]^{-1}, \tag{11}$$

where $\mathbf{d}(\mathbf{k}_{\parallel}) = v\mathbf{k}_{\parallel}a$ (with v specified in Supplementary Section H) couples the states with different parities in the σ bonding effective model, and a and c are the lattice constant along x or y and z, respectively. Other parameters in equation (11) are defined below equation (8). We mention that $\sum_{i=x,y} \sum_{\alpha}^{-} g_{\mathrm{eff},1,\alpha}(0)$ itself is not bounded from below since the σ bonding states at Γ are gapped. Instead, we look at the product of the gap squared and the OFSM, which is in dependent of the gap. In particular, by using the Hölder inequality, we find that the integration of $\sum_{i=x,y} \sum_{\alpha}^{-} \Delta E_{\mathrm{eff}}^2(0) [g_{\mathrm{eff},1,\alpha}(0)]_{ii}/|\mathbf{d}(\mathbf{k}_{\parallel})|^2$ on the Fermi surface is bounded from below by the winding number of $\mathbf{d}(\mathbf{k}_{\parallel})$. Since the winding number of $\mathbf{d}(\mathbf{k}_{\parallel})$ determines the change of the topological invariant caused by the band inversion at Γ , it is further bounded from below by the effective Euler number (see details in Supplementary Section H). As shown in Table 1, the total topological contribution $\lambda_{\mathrm{topo}} = \lambda_{\pi,\mathrm{topo}} + \lambda_{\sigma,\mathrm{topo}}$ is about 44% of the quantum geometric contribution λ_{geo} .

We note that the topological contribution just tells us that the geometric contribution may be stronger in the topologically non-trivial system. In principle, there can be trivial bands in real materials that have strong geometric properties and have a large geometric contribution.

Discussion

Our work shows that quantum geometric properties, now at the forefront of flat band research, are also fundamental—and can in fact be dominant-in a deep understanding of the different contributions to the EPC in systems with dispersive bands. One future direction is the development of a general framework that specifies the geometric and topological contributions to the bulk EPC constant λ for all two-dimensional (2D) and 3D systems with any types of topological invariants of states on or near Fermi surface. Our current results imply that, given two systems with similar band dispersion, the system with stronger geometric properties would tend to have a stronger EPC, which serves as guidance for future material search (for example, one could look for Weyl semi-metals that have Fermi surfaces enclosing Weyl points with large net chiralities). The study of the geometric and topological contributions to the bulk EPC constant *\lambda* in more phonon-mediated superconducting materials is essential for checking the relation between the electron band topology or geometry and the superconducting T_c . Further work will focus on an ab initio high-throughput calculation of the quantum geometry effects in the EPC of many other multi-band superconductors.

We find that the energetic contribution λ_E in graphene can be directly measured from the zero-temperature phonon line width of the E_{2g} phonons at Γ , together with the frequencies of the E_{2g} phonons at Γ and the A_1' phonon at K (Supplementary Section J). Experimentally, the frequency and line width of the E_{2g} phonons at Γ can be measured by Raman spectroscopy 52 , while the frequency of the A_1' phonon at K can be approximated by inelastic x-ray scattering measurements in graphite 53 . Existing experimental data suggest that the experimental value of λ_E for $\mu \approx -0.1$ eV is 0.0018-0.0034, whereas the value from our model is 0.0032, which is within the current experimental range. More precise measurements can be done in the future. Combined with the fact that the total λ of graphene may be measured from the Helium scattering 54 , the geometric contribution λ_{geo} may be measured from $\lambda - \lambda_E$. Furthermore, the FSM in graphene may be measured from the current noise spectrum 10 or more generally the first-order optical

response⁵⁵, owing to the two-band nature of graphene. Therefore, $\frac{\lambda_{\rm geo}}{\lambda_{\rm E}} = \frac{|\mu|}{\pi} \int_{\rm FS} {\rm d}\sigma_{\bf k} \frac{{\rm Tr}[g_{n_{\rm F}}({\bf k})]}{|\nabla_{\bf k} E_{n_{\rm F}}({\bf k})|} = \frac{\hbar c}{2\pi^2 {\rm e}^2} A(\omega = 2|\mu|/\hbar) \ {\rm may} \ {\rm be} \ {\rm experimentally}$

testable, where $A(\omega)$ is the optical absorption coefficient for photons with frequency ω in the unit system where $1/(4\pi\epsilon_0) = 1$, h is the Planck constant, c is the speed of light, e is the elementary charge, μ is the chemical potential and ε_0 is the vacuum permittivity. (ref. 55). If tested, this expression would relate the $\frac{\lambda_{\rm geo}}{\lambda_{\rm E}}$ in scattering experiments to the response coefficient in the optical response. Besides graphene, on the surface of the topological insulator Bi₂Se₃ with a hexagonal distortion⁵⁶, we can track the momentum dependence of the geometric quantities (such as the FSM and OFSM) and the EPC coupling measured in timeand angle-resolved photoemission spectroscopy measurements⁵⁷, as a test of the relation between quantum geometry and the EPC strength. For 3D materials such as MgB₂, the EPC constant λ can be measured in various ways, for example, by tracking the temperature behaviour of the specific heat⁵⁸ or inelastic x-ray scattering experiments⁴⁸. It is possible to test our theory in a system with tunable band geometry or topology by measuring the EPC constant while changing the band geometry or topology, for example, through gating in two dimensions or strain in three dimensions.

Note that, during the review process of this manuscript, ref. 59 (authored by one of the authors of the current work), which applied the GA proposed in this work to kagome ScV_6Sn_6 and explained the phonon softening in the system, was posted online.

Online content

Any methods, additional references, Nature Portfolio reporting summaries, source data, extended data, supplementary information, acknowledgements, peer review information; details of author contributions and competing interests; and statements of data and code availability are available at https://doi.org/10.1038/s41567-024-02486-0.

References

- Provost, J. & Vallee, G. Riemannian structure on manifolds of quantum states. Commun. Math. Phys. 76, 289 (1980).
- Resta, R. The insulating state of matter: a geometrical theory. Eur. Phys. J. B 79, 121 (2011).
- Bradlyn, B. et al. Topological quantum chemistry. Nature 547, 298–305 (2017).
- Lieb, E. H. Two theorems on the Hubbard model. *Phys. Rev. Lett.* 62, 1201 (1989).
- Mielke, A. Ferromagnetism in the Hubbard model on line graphs and further considerations. J. Phys. A 24, 3311 (1991).
- Călugăru, D. et al. General construction and topological classification of crystalline flat bands. Nat. Phys. 18, 185–189 (2022).
- Peotta, S. & Törmä, P. Superfluidity in topologically nontrivial flat bands. Nat. Commun. 6, 8944 (2015).
- Törmä, P., Peotta, S. & Bernevig, B. A. Superconductivity, superfluidity and quantum geometry in twisted multilayer systems. *Nat. Rev. Phys.* 4, 528–542 (2022).
- Hosur, P. Circular photogalvanic effect on topological insulator surfaces: Berry-curvature-dependent response. *Phys. Rev. B* 83, 035309 (2011).
- Neupert, T., Chamon, C. & Mudry, C. Measuring the quantum geometry of bloch bands with current noise. *Phys. Rev. B* 87, 245103 (2013).
- 11. Gao, Y., Yang, S. A. & Niu, Q. Field induced positional shift of bloch electrons and its dynamical implications. *Phys. Rev. Lett.* **112**, 166601 (2014).
- Morimoto, T. & Nagaosa, N. Topological nature of nonlinear optical effects in solids. Sci. Adv. 2, e1501524 (2016).
- de Juan, F., Grushin, A. G., Morimoto, T. & Moore, J. E. Quantized circular photogalvanic effect in Weyl semimetals. *Nat. Commun.* 8, 15995 (2017).

- Liang, L. et al. Band geometry, Berry curvature, and superfluid weight. Phys. Rev. B 95, 024515 (2017).
- Ozawa, T. & Goldman, N. Extracting the quantum metric tensor through periodic driving. Phys. Rev. B 97, 201117 (2018).
- Li, Y. & Haldane, F. D. M. Topological nodal Cooper pairing in doped Weyl metals. *Phys. Rev. Lett.* 120, 067003 (2018).
- Gao, Y. & Xiao, D. Nonreciprocal directional dichroism induced by the quantum metric dipole. *Phys. Rev. Lett.* 122, 227402 (2019).
- Gianfrate, A. et al. Measurement of the quantum geometric tensor and of the anomalous Hall drift. Nature 578, 381–385 (2020).
- Rhim, J.-W., Kim, K. & Yang, B.-J. Quantum distance and anomalous Landau levels of flat bands. Nature 584, 59–63 (2020).
- Kozii, V., Avdoshkin, A., Zhong, S. & Moore, J. E. Intrinsic anomalous Hall conductivity in a nonuniform electric field. *Phys. Rev. Lett.* 126, 156602 (2021).
- Chen, W. & Huang, W. Quantum-geometry-induced intrinsic optical anomaly in multiorbital superconductors. *Phys. Rev. Res.* 3, L042018 (2021).
- Ahn, J., Guo, G.-Y., Nagaosa, N. & Vishwanath, A. Riemannian geometry of resonant optical responses. *Nat. Phys.* 18, 290–295 (2022).
- 23. Bardeen, J., Cooper, L. N. & Schrieffer, J. R. Theory of superconductivity. *Phys. Rev.* **108**, 1175 (1957).
- 24. Migdal, A. Interaction between electrons and lattice vibrations in a normal metal. Sov. Phys. JETP 7, 996 (1958).
- 25. Eliashberg, G. Interactions between electrons and lattice vibrations in a superconductor. Sov. Phys. JETP 11, 696 (1960).
- McMillan, W. L. Transition temperature of strong-coupled superconductors. *Phys. Rev.* 167, 331 (1968).
- Allen, P. B. & Dynes, R. C. Transition temperature of strong-coupled superconductors reanalyzed. *Phys. Rev. B* 12, 905 (1975).
- 28. Vergniory, M. G. et al. A complete catalogue of high-quality topological materials. *Nature* **566**, 480–485 (2019).
- Zhang, T. et al. Catalogue of topological electronic materials. Nature 566, 475–479 (2019).
- 30. Tang, F., Po, H. C., Vishwanath, A. & Wan, X. Comprehensive search for topological materials using symmetry indicators. *Nature* **566**, 486–489 (2019).
- Baroni, S., de Gironcoli, S., Dal Corso, A. & Giannozzi, P. Phonons and related crystal properties from density-functional perturbation theory. Rev. Mod. Phys. 73, 515 (2001).
- Nagamatsu, J., Nakagawa, N., Muranaka, T., Zenitani, Y. & Akimitsu,
 J. Superconductivity at 39 K in magnesium diboride. *Nature* 410,
 63–64 (2001).
- Bud'ko, S. L. et al. Boron isotope effect in superconducting mgb₂. Phys. Rev. Lett. 86, 1877 (2001).
- Hinks, D. G., Claus, H. & Jorgensen, J. D. The complex nature of superconductivity in MgB₂ as revealed by the reduced total isotope effect. *Nature* 411, 457–460 (2001).
- Esterlis, I. et al. Breakdown of the Migdal–Eliashberg theory: a determinant quantum Monte Carlo study. *Phys. Rev. B* 97, 140501 (2018).
- Sous, J., Chakraborty, M., Krems, R. V. & Berciu, M. Light bipolarons stabilized by peierls electron-phonon coupling. *Phys. Rev. Lett.* 121, 247001 (2018).
- 37. Mitra, T. Electron-phonon interaction in the modified tight-binding approximation. *J. Phys. C* **2**, 52 (1969).
- Törmä, P., Liang, L. & Peotta, S. Quantum metric and effective mass of a two-body bound state in a flat band. *Phys. Rev. B* 98, 220511 (2018).
- 39. Castro Neto, A. H., Guinea, F., Peres, N. M. R., Novoselov, K. S. & Geim, A. K. The electronic properties of graphene. *Rev. Mod. Phys.* **81** 109 (2009)
- Tarnopolsky, G., Kruchkov, A. J. & Vishwanath, A. Origin of magic angles in twisted bilayer graphene. *Phys. Rev. Lett.* 122, 106405 (2019).

- 41. Bernevig, B. A., Song, Z.-D., Regnault, N. & Lian, B. Twisted bilayer graphene. III. Interacting Hamiltonian and exact symmetries. *Phys. Rev. B* **103**, 205413 (2021).
- 42. Song, Z.-D. & Bernevig, B. A. Magic-angle twisted bilayer graphene as a topological heavy fermion problem. *Phys. Rev. Lett.* **129**, 047601 (2022).
- 43. Liu, C.-X., Chen, Y., Yazdani, A. & Bernevig B. A. Electron–K-phonon interaction in twisted bilayer graphene. Preprint at https://arxiv.org/abs/2303.15551 (2023).
- 44. Cao, Y. et al. Unconventional superconductivity in magic-angle graphene superlattices. *Nature* **556**, 43–50 (2018).
- Kortus, J., Mazin, I. I., Belashchenko, K. D., Antropov, V. P. & Boyer, L. L. Superconductivity of metallic boron in MgB₂. Phys. Rev. Lett. 86, 4656 (2001).
- 46. An, J. M. & Pickett, W. E. Superconductivity of MgB₂: covalent bonds driven metallic. *Phys. Rev. Lett.* **86**, 4366 (2001).
- Kong, Y., Dolgov, O. V., Jepsen, O. & Andersen, O. K. Electronphonon interaction in the normal and superconducting states of MgB₂. Phys. Rev. B 64, 020501 (2001).
- 48. Shukla, A. et al. Phonon dispersion and lifetimes in MgB₂. *Phys. Rev. Lett.* **90**, 095506 (2003).
- 49. Jin, K.-H. et al. Topological superconducting phase in high- T_c superconductor MgB₂ with Dirac-nodal-line fermions. *npj* Comput. Mater. **5**, 57 (2019).
- 50. Aroyo, M. I. et al. Bilbao crystallographic server: I. databases and crystallographic computing programs. *Z. Kristallogr. Cryst. Mater.* **221**, 15 (2006).
- 51. Ahn, J., Park, S. & Yang, B.-J. Failure of Nielsen–Ninomiya theorem and fragile topology in two-dimensional systems with space–time inversion symmetry: application to twisted bilayer graphene at magic angle. *Phys. Rev. X* **9**, 021013 (2019).
- 52. Yan, J., Zhang, Y., Kim, P. & Pinczuk, A. Electric field effect tuning of electron–phonon coupling in graphene. *Phys. Rev. Lett.* **98**, 166802 (2007).
- Maultzsch, J., Reich, S., Thomsen, C., Requardt, H. & Ordejón, P. Phonon dispersion in graphite. *Phys. Rev. Lett.* 92, 075501 (2004).
- 54. Zhu, X. et al. Electron-phonon coupling on the surface of the topological insulator Bi₂Se₃ determined from surface-phonon dispersion measurements. *Phys. Rev. Lett.* **108**, 185501 (2012).
- 55. Sipe, J. E. & Shkrebtii, A. I. Second-order optical response in semiconductors. *Phys. Rev. B* **61**, 5337 (2000).
- Chen, Y. et al. Experimental realization of a three-dimensional topological insulator, Bi2Te3. Science 325, 178 (2009).
- 57. Hatch, R. C. et al. Stability of the Bi₂Se₃(111) topological state: electron–phonon and electron–defect scattering. *Phys. Rev. B* **83**, 241303 (2011).
- Wang, Y., Plackowski, T. & Junod, A. Specific heat in the superconducting and normal state (2–300 K, 0–16 T), and magnetic susceptibility of the 38 K superconductor MgB₂: evidence for a multicomponent gap. *Physica C* 355, 179 (2001).
- 59. Korshunovet, A. et al. Softening of a flat phonon mode in the kagome ScV₆Sn₆. *Nat. Commun.* **14**, 6646 (2023).

Publisher's note Springer Nature remains neutral with regard to jurisdictional claims in published maps and institutional affiliations.

Springer Nature or its licensor (e.g. a society or other partner) holds exclusive rights to this article under a publishing agreement with the author(s) or other rightsholder(s); author self-archiving of the accepted manuscript version of this article is solely governed by the terms of such publishing agreement and applicable law.

© The Author(s), under exclusive licence to Springer Nature Limited 2024

Data availability

The datasets generated during and/or analysed during the current study are available from the authors on reasonable request. Source data are provided with this paper.

Code availability

The code generated during and/or analysed for the current study is available from the authors on reasonable request.

Acknowledgements

We acknowledge E. Baldini, D. Calugaru, M. Cheng, S. Das Sarma, L. Glazman, F. D. M. Haldane, J. Herzog-Arbeitman, H. Hu, L.-H. Hu, Y. H. Kwan, B. Lian, C.-Hwan Park, Z.-D. Song, I. Souza, J. Sous, X.-Q. Sun, P. Törmä, Y. Xu, R.-X. Zhang and especially C.-X. Liu for helpful discussion. B.A.B.'s research was supported by the European Research Council under the European Union's Horizon 2020 research and innovation programme (grant agreement no. 101020833) and partially by the Simons Investigator grant no. 404513, the Gordon and Betty Moore Foundation through grant no. GBMF8685 towards the Princeton theory programme, the Gordon and Betty Moore Foundation's EPiQS Initiative (grant no. GBMF11070), the Office of Naval Research (grant no. N00014-20-1-2303), the Global Collaborative Network Grant at Princeton University, the BSF Israel-US Foundation (no. 2018226) and the NSF-MERSEC (grant no. MERSEC DMR 2011750). J.Y. is supported by the Gordon and Betty Moore Foundation through grant no. GBMF8685 toward the Princeton theory programme. I.E. and B.A.B. are part of the SuperC collaboration. I.E. has received funding from the European Research Council under the European Union's Horizon 2020 research and innovation programme (grant agreement no. 802533) and the Department of Education, Universities and Research

of the Eusko Jaurlaritza and the University of the Basque Country UPV/EHU (grant no. IT1527-22). Calculations by C.J.C. and P.N. were supported by Office of Naval Research grant no. 13672292 and by Gordon and Betty Moore Foundation grant no. 8048. P.N. gratefully acknowledges support from the Alexander von Humboldt Foundation (Bessel Research Award) and from the John Simon Guggenheim Memorial Foundation (Guggenheim Fellowship).

Author contributions

J.Y. and B.A.B. conceived and supervised the project. J.Y. and B.A.B. performed the theoretical analysis. C.J.C., R.B., I.E. and P.N. performed the ab initio calculations. J.Y. and B.A.B. wrote the paper, with input from C.J.C., R.B., I.E. and P.N.

Competing interests

The authors declare no competing interests.

Additional information

Supplementary information The online version contains supplementary material available at https://doi.org/10.1038/s41567-024-02486-0.

Correspondence and requests for materials should be addressed to B. Andrei Bernevig.

Peer review information *Nature Physics* thanks the anonymous reviewers for their contribution to the peer review of this work.

Reprints and permissions information is available at www.nature.com/reprints.